Article

The Organization of Somatostatin-Immunoreactive Cells in the Visual Cortex of the Gerbil

Kyung-Min Kwon [1,2,†], Myung-Jun Lee [1,†], Han-Saem Chung [3], Jae-Hong Pak [2,3] and Chang-Jin Jeon [1,2,*]

[1] Department of Biology, School of Life Sciences, BK21 FOUR KNU Creative Bio-Research Group, College of Natural Sciences, Brain Science and Engineering Institute, Kyungpook National University, Daegu 41566, Korea; us3469@knu.ac.kr (K.-M.K.); bridlee900@knu.ac.kr (M.-J.L.)

[2] Research Institute for Dok-do and Ulleung-do Island, Department of Biology, School of Life Sciences, Kyungpook National University, 80 Daehak-ro, Buk-gu, Daegu 41566, Korea; jhpak@knu.ac.kr

[3] Department of Biology, School of Life Sciences, College of Natural Sciences, Kyungpook National University, Daegu 41566, Korea; 2018117591@knu.ac.kr

[*] Correspondence: cjjeon@knu.ac.kr

[†] These authors contributed equally to this work.

Abstract: Somatostatin (SST) is widely expressed in the brain and plays various, vital roles involved in neuromodulation. The purpose of this study is to characterize the organization of SST neurons in the Mongolian gerbil visual cortex (VC) using immunocytochemistry, quantitative analysis, and confocal microscopy. As a diurnal animal, the Mongolian gerbil provides us with a different perspective to other commonly used nocturnal rodent models. In this study, SST neurons were located in all layers of the VC except in layer I; they were most common in layer V. Most SST neurons were multipolar round/oval or stellate cells. No pyramidal neurons were found. Moreover, 2-color immunofluorescence revealed that only 33.50%, 24.05%, 16.73%, 0%, and 64.57% of SST neurons contained gamma-aminobutyric acid, calbindin-D28K, calretinin, parvalbumin, and calcium/calmodulin-dependent protein kinase II, respectively. In contrast, neuropeptide Y and nitric oxide synthase were abundantly expressed, with 80.07% and 75.41% in SST neurons, respectively. Our immunocytochemical analyses of SST with D_1 and D_2 dopamine receptors and choline acetyltransferase, α_7 and β_2 nicotinic acetylcholine receptors suggest that dopaminergic and cholinergic fibers contact some SST neurons. The results showed some distinguishable features of SST neurons and provided some insight into their afferent circuitry in the gerbil VC. These findings may support future studies investigating the role of SST neurons in visual processing.

Keywords: somatostatin; visual cortex; gamma-aminobutyric acid; calcium-binding proteins; calcium/calmodulin-dependent protein kinase II; dopamine receptors; nicotinic cholinergic receptors; Mongolian gerbil; immunocytochemistry

1. Introduction

Somatostatin (SST), first isolated from the ovine hypothalamus in 1973, acts as a growth hormone inhibitory peptide [1]. SST impacts a wide variety of physiological functions, such as hormonal regulation [1,2], gastrointestinal regulation [3], plasticity [4–6], learning [5,7], memory [6], and visual processing [8–10]. Pathologically, SST is involved in multiple diseases, such as schizophrenia [11], Alzheimer's disease [6], depression [12], and obesity [13].

The identification of the transmitter-, neuromodulator-, and peptide-specific heterogenous types of neurons is essential to understanding the brain's functioning. In the cerebral cortex, SST neurons constitute a large cortical subpopulation of interneurons, comprising approximately 30% of gamma-aminobutyric acid (GABA)ergic interneurons [14–16]. Three major EF-hand calcium-binding proteins (CBPs), calbindin-D28K (CB), calretinin (CR), and parvalbumin (PV), have been extensively utilized to localize different types of cortical

interneurons and SST neurons [17–20]. Two additional markers have been used to identify interneuron subtypes and have been known to have overlapping populations with SST neurons: neuropeptide Y (NPY) and nitric oxide synthase (NOS). NPY, one of the most abundantly expressed neuropeptides in the brain, is mostly seen in GABAergic neurons. NOS produces a retrograde neurotransmitter, nitric oxide [21–25].

Similarly to the somatosensory and auditory cortex, the visual cortex (VC) is composed of six distinct cortical layers that are characterized by their synaptic in- and out-puts and by specific cell types present in each layers [26]. The major class of projection neurons in the VC is the heterogenous types of pyramidal cells which are located in any of the cortical layers except layer I. Extremely large number of genetic, functional and/or structural types of cortical interneurons have been identified [26–30]. In this study, we focused on SST neurons that are specifically found in cortical layers II/III and V/VI. SST neurons have been identified in the VC of various animals including mammals and non-mammals, such as monkeys [31,32], cats [33–37], rabbits [38], rats [31,39–43], mice [14], pigeon visual Wulst [44], and the squid optic lobe [45]. The majority of SST neurons in the mammalian VC are non-pyramidal interneurons [14,32,34,35,39–41,46,47]. The cortical distribution of SST neurons varies with animal species, but they are generally concentrated in either layer II/III [32,38,40,42,43] or V/VI [32,34,37,41].

Mongolian gerbils, *Meriones unguiculatus*, are rodents belonging to the subfamily Gerbillinae. Gerbils are widely used as research models in areas such as aging [48], metabolism [49–54], anatomy [55,56], and parasitic diseases [57,58]. In neuroscience research, gerbils have been widely used to study sensory systems [59–63], neural diseases [61,64–66], and brain structure [67–69]. Mice and rats are common in biomedical and neuroscience research due to their genetic manipulability and well-published data. However, gerbils are particularly important and have specific advantages for studies on the central visual system. For example, mice and rats are nocturnal animals with rod-dominated retinae. Gerbils, however, are diurnal animals with a higher proportion of retinal cones compared to mice and rats [70–72], thus giving them a higher visual acuity [73]. Furthermore, gerbils have a specialized retinal region, which is similar to the human fovea [72,74]. Accordingly, gerbils have been used widely in studies of the central visual system, such as the retina [71,72,75,76] and sensory cortex, including the VC [61–63,77].

Although SST neurons have been extensively examined in various animals, the neuronal architecture of SST neurons has not been studied in the Mongolian gerbil VC. Pursuing this knowledge of such an excellent animal model holds important implications for central visual system research. Therefore, we have designed this study to investigate the organization of SST neurons in the gerbil VC.

It is well known that the morphological identification of neurons is a direct reflection of their functional connection and, thus, provides a fundamental understanding of the brain. Therefore, we first examined the distribution and morphology of SST neurons to identify any heterogenous subtypes. Next, we determined the expression patterns of GABA in SST neurons to determine any species differences. Then, as cell types can be distinguished by the expression of specific peptides, we determined different expression patterns of various CBPs, NPY, and NOS in SST neurons. Finally, although some outputs of SST neurons have been studied in detail, little is known about the synaptic inputs into these cells; hence, we decided to analyze dopaminergic and cholinergic receptors in SST neurons. Both dopamine [78,79] and SST [80] are known to play a role in mood regulation. It is also known that cholinergic signaling through neuronal nicotinic acetylcholine receptors (nAChRs) modulates higher cognitive functions [81], including memory [82]. Interestingly, SST neurons also contribute to cognition [8] and memory formation [6]. Our results show diverse heterogenous types of SST neurons based on varying morphologies and expressional patterns of GABA, CBPs, NPY, and NOS. We also provide evidence to suggest possible connections of SST neurons with dopaminergic and cholinergic neurons.

2. Materials and Methods

2.1. Animal and Tissue Preparation

A total of 15 adult Mongolian gerbils (*Meriones unguiculatus*) (aged 3–4 months, weighing 70–90 g), obtained from a local vendor, were used in this study. Animals were group housed under a 12 h light:12 h dark cycle until used for the study. The temperature and humidity in the facilities ranged from 23 to 26 °C and from 45 to 65%, respectively. All of the animals were deeply anesthetized with isoflurane (5% in O_2) and perfused intracardially with 4% paraformaldehyde and 0.3% glutaraldehyde in 0.1 M sodium phosphate buffer (pH 7.4) containing 0.002% $CaCl_2$. Procedures for perfusion, isolation of the brain and tissue sectioning were based on those previously described [83–85]. The Guide for the Care and Use of Laboratory Animals (https://grants.nih.gov/grants/olaw/guide-for-the-care-and-use-of-laboratory-animals.pdf; accessed on 20 October 2021) was followed. All of the animal experiments were approved by the Animal Care and Use Committee of Kyungpook National University (permission NO. 2014-0181).

2.2. Horseradish Peroxidase Staining

Monoclonal rat anti-SST was used as the primary antibody and biotinylated anti-rat IgG produced in goats was used as the secondary antibody (Table 1). Both antibodies were diluted at a ratio of 1:200. Standard immunocytochemical techniques and methods were used, as previously described [83,84]. As a negative control, some sections were incubated in the same solution without the addition of the primary antibody. These control tissues showed no SST immunoreactivity. The final sections were examined and photographed on a Zeiss Axioplan microscope (Carl Zeiss Meditec, Inc., Jena, Germany) with conventional or differential interference contrast (DIC) optics.

2.3. Fluorescence Immunocytochemistry

Standard immunocytochemical methods were employed as described earlier [83–85]. Cortical sections were double-labeled for SST with each of the following: GABA, CBPs (CB, CR, PV), NPY, NOS, CaMKII, and D_1 or D_2 dopamine receptors. Triple-labels were conducted on sections for SST, choline acetyltransferase (ChAT), and α_7 or β_2 nAChRs. Labeled sections were preserved under coverslips in Vectashield mounting medium (Vector Laboratories, Inc., Burlingame, CA, USA). The complete information of the primary and secondary antibodies used is listed in Table 1.

2.4. Quantitative Analysis

All of the methods have been described in detail elsewhere and are only summarized here [85]. For the quantitative analysis of laminar distribution, a total of 9 sections, with a width of 2000 μm each, were sampled from each of the 3 animals (3 tissue sections per animal). The morphological types were analyzed for 558 neurons from 9 sections in 3 gerbils. The average diameter and area of SST neurons were determined for 202 neurons analyzed from 20 sections in 3 gerbils. Double-labeled neurons were counted from a total of 9 different tissue sections from each of the 3 animals, each 2000 μm in width, across all layers.

2.5. Synaptic Identification

Triple-labeling of SST neurons with ChAT-immunoreactive (IR) fibers and nAChRs was captured using a Zeiss LSM800 laser scanning confocal microscope (Carl Zeiss Meditec, Inc.) with a 100× objective. At the contact point between the SST neurons, ChAT-IR fibers, and receptors, z-series images of these 3 components were taken at 0.2 μm intervals along the z-axis using the same laser scanning confocal microscope. The images were viewed using an EC Plan-Neofluar 10×, C-Apochromat 40×/1.2 W, and/or 100×/1.2 oil, with objectives at 2.5× zoom. We obtained approximately 70–80 confocal images at the presumed synaptic contact. The z-series of the confocal images were reconstructed as three-dimensional (3D) images using the ZEN imaging software (2.3 blue edition service

pack 1, Carl Zeiss Microscopy GmbH, Jena, Germany). The 3D images and orthogonal views (xy, xz, and yz planes) were used to identify points where the ChAT-IR fibers and α_7 or β_2 nAChRs contacted the SST neurons.

Table 1. List of primary and secondary antibodies and their dilution used in present study.

Primary	Type	Dilution	Manufacturer
SST	RtM	1:200	Millipore, Burlington, MA, USA
GABA	MM	1:500	Millipore
CB	MM	1:500	Sigma-Aldrich, Saint Louis, MO, USA
CR	MM	1:500	Sigma-Aldrich
CR	RbP	1:100	Sigma-Aldrich
PV	MM	1:500–1000	Millipore
NPY	RbP	1:500	Immunostar, Hudson, WI, USA
NOS	MM	1:200	BD Biosciences, San Jose, CA, USA
CaMKII	RbP	1:500	Proteintech, Rosemont, IL, USA
D_1	MM	1:200	Santa Cruz Biotechnology, Inc., Dallas, TX, USA
D_2	MM	1:200	Santa Cruz Biotechnology, Inc.
ChAT	MM	1:250	Millipore
α_7	RbP	1:200	Santa Cruz Biotechnology, Inc.
β_2	RbP	1:200	Santa Cruz Biotechnology, Inc.

Secondary	Conjugation	Dilution	Target	Manufacturer
HRP				
Goat anti-rat IgG	Biotinylated	1:200	SST	Vector laboratories, Inc., Burlingame, CA, USA
Fluorescence				
Goat anti-rat IgG	Cy3	1:200	SST	Jackson ImmunoResearch Laboratories, Inc., West Grove, PA, USA
Horse anti-mouse IgG	FITC	1:200	CB, CR(MM), PV, GABA, ChAT, D_1, D_2, NOS	Vector laboratories, Inc.
Goat anti-rabbit IgG	FITC	1:200	CR(RbP), NPY, CaMKII	Jackson ImmunoResearch Laboratories, Inc.
Goat anti-rabbit IgG	Cy5	1:200	α_7, β_2	Jackson ImmunoResearch Laboratories, Inc.

SST, somatostatin; GABA, gamma-aminobutyric acid; CB, calbindin-D28K; CR, calretinin; PV, parvalbumin; NPY, neuropeptide Y; NOS, nitric oxide synthase; CaMKII, calcium/calmodulin-dependent protein kinase II; D_1, D_1 dopamine receptor; D_2, D_2 dopamine receptor; ChAT, choline acetyltransferase; α_7, α_7 nicotinic acetylcholine receptor; β_2, β_2 nicotinic acetylcholine receptor; RtM, rat monoclonal; MM, mouse monoclonal; RbP, rabbit polyclonal.

3. Results

3.1. Laminar Distribution of SST Neurons

SST neurons were selectively distributed in the gerbil VC (Figure 1). Figure 1A shows a thionin-stained section of a gerbil VC, which revealed division of the cortical layers. Figure 1B shows the laminar distribution of SST neurons with different intensities of staining. The first group of neurons were intensely stained (Figure 1B, arrowheads). These intensely stained neurons were mostly located in layers V–VI and sparsely distributed through II–IV (Figure 1D, black colored bars). The second group of neurons were weakly stained (Figure 1B, arrows), and these types of neurons showed a more even distribution compared to the former group (Figure 1D, white colored bars). In both groups, the distribution peaked at layer V and was absent in layer I, except a single weakly stained SST neuron found in layer I. Figure 1C represents a dark field image of SST fibers forming a plexus throughout multiple layers. Figure 1D shows the relative frequency of the laminar distribution of the two differently stained SST neurons and the sum of both calculated SST neurons, respectively. Quantitatively, 0% ± 0% (mean ± S.D.) of intensely stained SST neurons were

found in layer I, 3.50% ± 3.96% were found in layer II, 6.29% ± 4.32% were found in layer III, 2.10% ± 3.47% were found in layer IV, 51.05% ± 21.2% were found in layer V, and 37.06% ± 19.54% were found in layer VI. Furthermore, 0.17% ± 0.54% of weakly stained SST neurons were found in layer I, 7.20% ± 3.03% were found in layer II, 24.01% ± 6.58% were found in layer III, 25.73% ± 6.57% were found in layer IV, 30.53% ± 4.35% were found in layer V, and 12.35% ± 4.34% were found in layer VI. 0.14% ± 0.44% of total SST neurons were found in layer I, 6.47% ± 2.41% were found in layer II, 20.52% ± 8.41% were found in layer III, 21.07% ± 4.71% were found in layer IV, 34.57% ± 4.78% were found in layer V, and 17.22% ± 4.49% were found in layer VI (Figure 1D, striped bars).
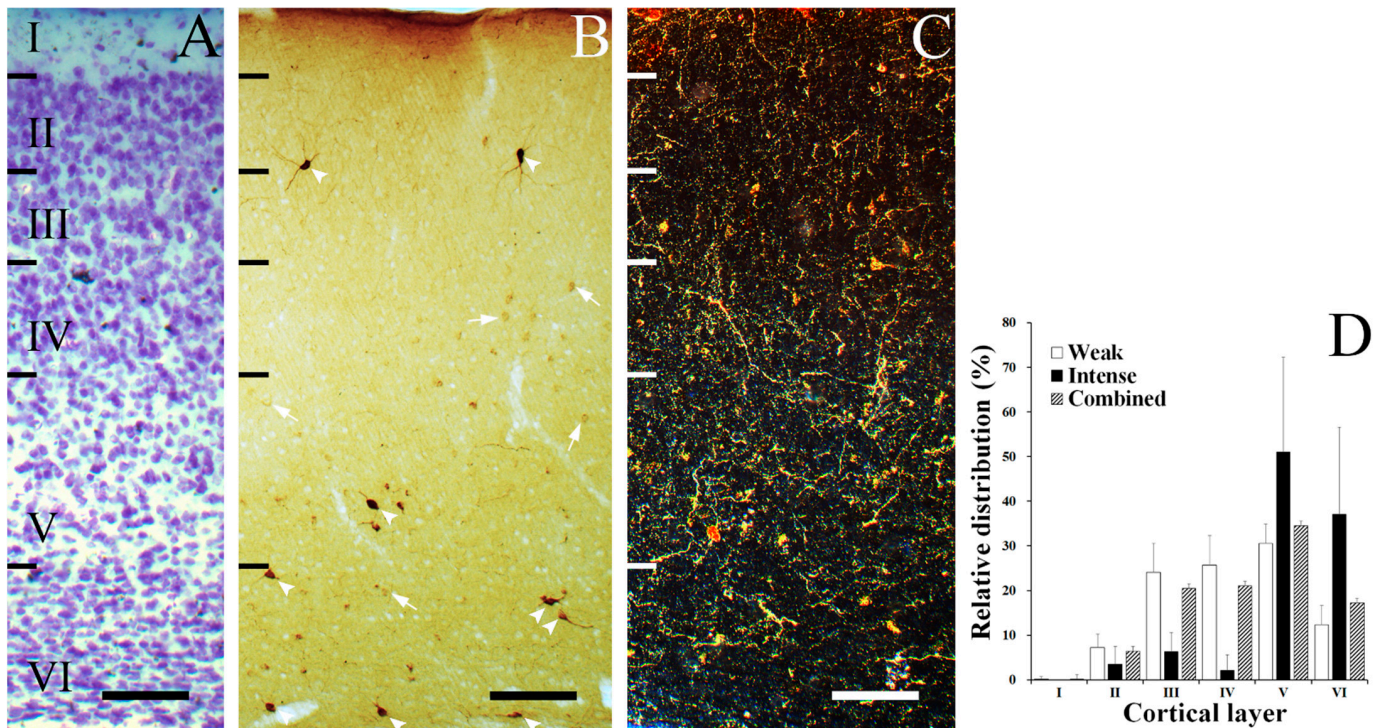

Figure 1. Laminar distribution of SST neurons in the gerbil VC. (**A**) Thionin-stained section illustrating the layer division in gerbil VC. (**B**) Immunostained section showing distribution of SST neurons in gerbil VC. SST neurons in gerbil VC can be distinguished as either intensely (arrowheads) or weakly (arrows) stained, based on their intensity of staining. (**C**) Low-magnification dark field photomicrograph of the gerbil VC with SST fibers dispersed throughout whole layers. (**D**) Histogram of the relative distribution of intensely and weakly stained SST neurons in the gerbil VC. The error bars represent standard deviation (S.D.). Scale bar = 100 μm.

3.2. Morphology of SST Neurons

Figure 2A–J show the representative form of each cell type. Figure 2A,B,G represent multipolar round/oval cells, the most common type in SST neurons, which have a round/oval-shaped cell body and multiple dendrites extending from the cell body to many directions. The multipolar round/oval cells had medium dendritic fields (200–300 μm in diameter). Figure 2C,D,H show multipolar stellate cells, which are the second most common type among SST neurons. Similarly to round/oval cells, these types of cells also have multiple dendrites proceeding to various directions. However, the polygonal-shaped cell body distinguishes these cells from round/oval cells. In general, the multipolar stellate cells had larger dendritic fields (300–400 μm in diameter) than round/oval cells. Figure 2E,I show typical vertical fusiform cells. These cells have a vertical fusiform cell body with two main processes, each ascending towards the pial surface and descending to lower layers, respectively. These types of cells have medium to large dendritic fields (200–400 μm in diameter). Figure 2F,J are examples of horizontal cells, which have a horizontally oriented

fusiform cell body and horizontally oriented long dendrites. In the present study, some fibers in this cell type were found to have more than 500 µm-long fibers (Figure 2J). Although a large amount of the SST-staining in the present study is notable, we still face the high possibility of a lack of complete staining of cells due to the limitations of immunocytochemistry, and truncations of some cell processes due to the sectioning and curving of processes. Thus, the labeling of dendrites was not sufficiently extensive to provide full descriptions of the dendritic size and morphology.
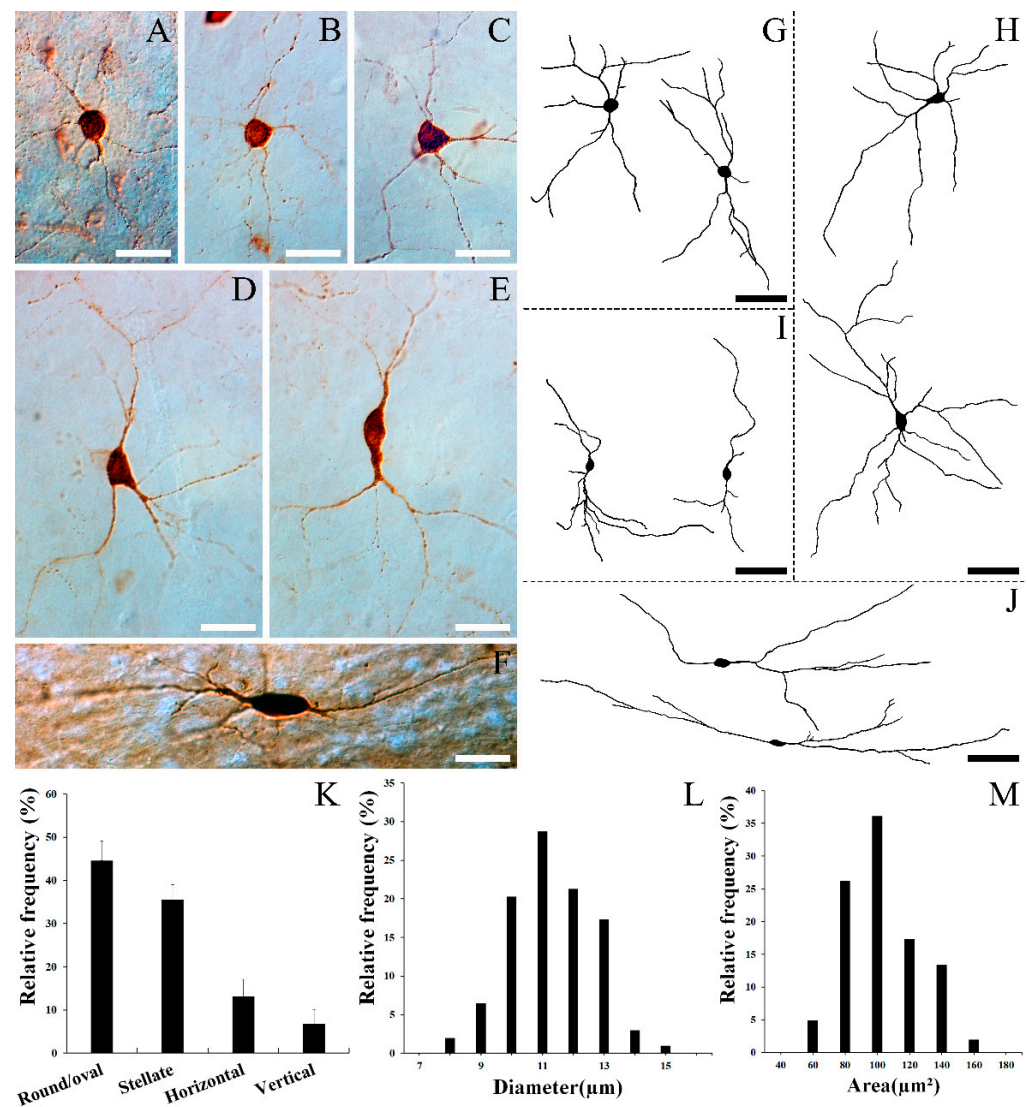

Figure 2. Images of SST neurons' morphologies and quantitative data in the gerbil VC. DIC photomicrographs (**A–F**) and drawings (**G–J**). (**A,B,G**) Multipolar round/oval cell. (**C,D,H**) Multipolar stellate cell. (**E,I**) Vertical fusiform cell. (**F,J**) Horizontal cell. Although the drawings are copies based on the best-stained cells, note that cell depictions may not be realistic due to the limitations of immunocytochemistry, such as imperfect filling of the whole cell body and trimming of fibers. (**K**) Histogram of the morphological distribution of SST neurons in the gerbil VC. Multipolar round/oval cells were the most commonly found. The average diameter (**L**) and area (**M**) of SST neurons in the gerbil VC were calculated. The average diameter ranged from 7.50 to 14.48 µm, with a mean of 10.81 µm (S.D. = 1.34). The average area of these cells ranged from 44.20 to 153.12 µm², with a mean of 93 µm² (S.D. = 22.70). The error bars represent standard deviation (S.D.). Scale bar = 20 (**A–F**) and 50 µm (**G–J**).

Figure 2K reveals the relative frequency of each cell type in the gerbil VC. Quantitatively, 44.62% ± 3.94% (mean ± S.D.) (249 of 558 cells) of SST neurons were round/oval,

35.48% ± 3.44% (198 of 558 cells) were stellate, 13.08% ± 3.98% (73 of 558 cells) were horizontal, and 6.81% ± 3.09% (38 of 558 cells) were vertical fusiform. Figure 2 shows the average diameter (O) and area (P) of SST neurons, respectively. The average diameter of SST neurons ranged from 7.50 to 14.48 μm, with a mean of 10.81 μm (S.D. = 1.34 μm). The vast majority of SST neurons (87.62%, 177 of 202 cells) had a diameter ranging between 9 to 13 μm, and none of these cells had a diameter > 15 μm. The area of these cells ranged from 44.20 to 153.12 μm^2, with a mean of 93.00 μm^2 (S.D. = 22.70 μm^2).

3.3. Colocalization of SST with GABA, CBPs, NOS, NPY, CaMKII, Dopamine Receptors, and ChAT with nAChRs

In the present study, we investigated whether the SST neurons in the gerbil VC colocalize with GABA, CBPs, NPY, or NOS. Figure 3 shows neurons stained with SST (Figure 3(A1,B1,C1,D1,E1,F1,G1,H1,I1,J1,K1)), GABA (Figure 3(A2,B2)), CBPs (Figure 3 (C2,D2,E2,F2,G2)), NPY (Figure 3(H2,I2)), NOS (Figure 3(J2,K2)), or CaMKII (Figure 3 (L2,M2)), and the overlapped images of SST with GABA (Figure 3(A3,B3)), CBPs (Figure 3 (C3,D3,E3,F3,G3)), NPY (Figure 3(H3,I3)), NOS (Figure 3(J3,K3)), or CaMKII (Figure 3 (L3,M3)). Some cells were clearly labeled with SST and GABA, CB, CR, NPY, NOS, or CaMKII antibodies in the gerbil VC. Other cells were labeled with one of the antibodies, but not both. There was no obvious relationship between cell morphology and whether the cell was single or double-labeled. None of the SST neurons were labeled with PV (Figure 3(G1–G3)). Quantitatively, 33.50% ± 6.04% (66 of 197 cells) of SST neurons were double-labeled with GABA, 24.05% ± 3.73% (51 of 212 cells) with CB, 16.73% ± 2.77% (40 of 239 cells) with CR, 0% (0 of 193 cells) with PV, 75.41% ± 8.64% (200 of 265 cells) with NOS, 80.07% ± 7.80% (217 of 271 cells) with NPY, and 64.57% ± 8.77% (164 of 254 cells) with CaMKII. The percentage of double-labeled cells was relatively consistent across sections and among animals (Table 2).

To determine if SST neurons in the gerbil VC receive synaptic inputs from dopaminergic neurons, we double-labeled them with D_1 or D_2 dopamine receptors. Figure 4 shows the double-labeling of SST neurons (red) with well-stained immunopuncta of D_1 or D_2 dopamine receptors (green). Some neurons were clearly co-labeled with anti-SST and anti-receptor antibodies. The immunopuncta of D_1 (Figure 4A,B) or D_2 (Figure 4C,D) dopamine receptors clearly surrounded some SST neurons (D_1 in Figure 4(A2,B2) or D_2 in Figure 4(C2,D2)). There were some cells (arrowhead) that were not surrounded with dopamine receptors or labeled with SST. Conversely, some cells (arrows) were surrounded by dopamine receptors but were not labeled with SST.

In order to identify whether SST neurons in the gerbil VC receive synaptic inputs from cholinergic neurons, we triple-labeled with them ChAT and either α_7 or β_2 nAChRs. Figure 5 shows the distribution of SST neurons (Figure 5A,H), ChAT-IR fibers (Figure 5B,I), α_7 nAChR (Figure 5C), and β_2 nAChR (Figure 5J). Merged images of the cell with fibers and each receptor are shown in Figure 5D,K. The crosshair reveals the colocalization of SST neurons and ChAT-IR fibers with the nAChRs, in an orthogonal projection. The areas marked with white squares in Figure 5A–D,H–K are displayed at higher magnification in Figure 5(E1–G4,L1–N4). The merged images of SST neurons and ChAT-IR fibers in the xy, xz, and yz planes are shown in Figure 5(E1,F1,G1,L1,M1,N1), respectively. Both SST neurons and ChAT-IR fibers are labeled together in every plane. This indicates the coexistence of the SST neurons and ChAT-IR fibers. Similarly, we identified that SST neurons and α_7 nAChRs (Figure 5(E2,F2,G2)); ChAT-IR fibers and α_7 nAChRs (Figure 5(E3,F3,G3)); SST neurons, ChAT-IR fibers, and α_7 nAChRs (Figure 5(E4,F4,G4)); SST neurons and β_2 nAChRs (Figure 5(L2,M2,N2)); ChAT-IR fibers and β_2 nAChRs (Figure 5(L3,M3,N3)); and SST neurons, ChAT-IR fibers, and β_2 nAChRs (L4,M4,N4) overlap in all 3 planes. These images suggest that cholinergic fibers make synaptic contacts and innervate SST neurons in the gerbil VC.
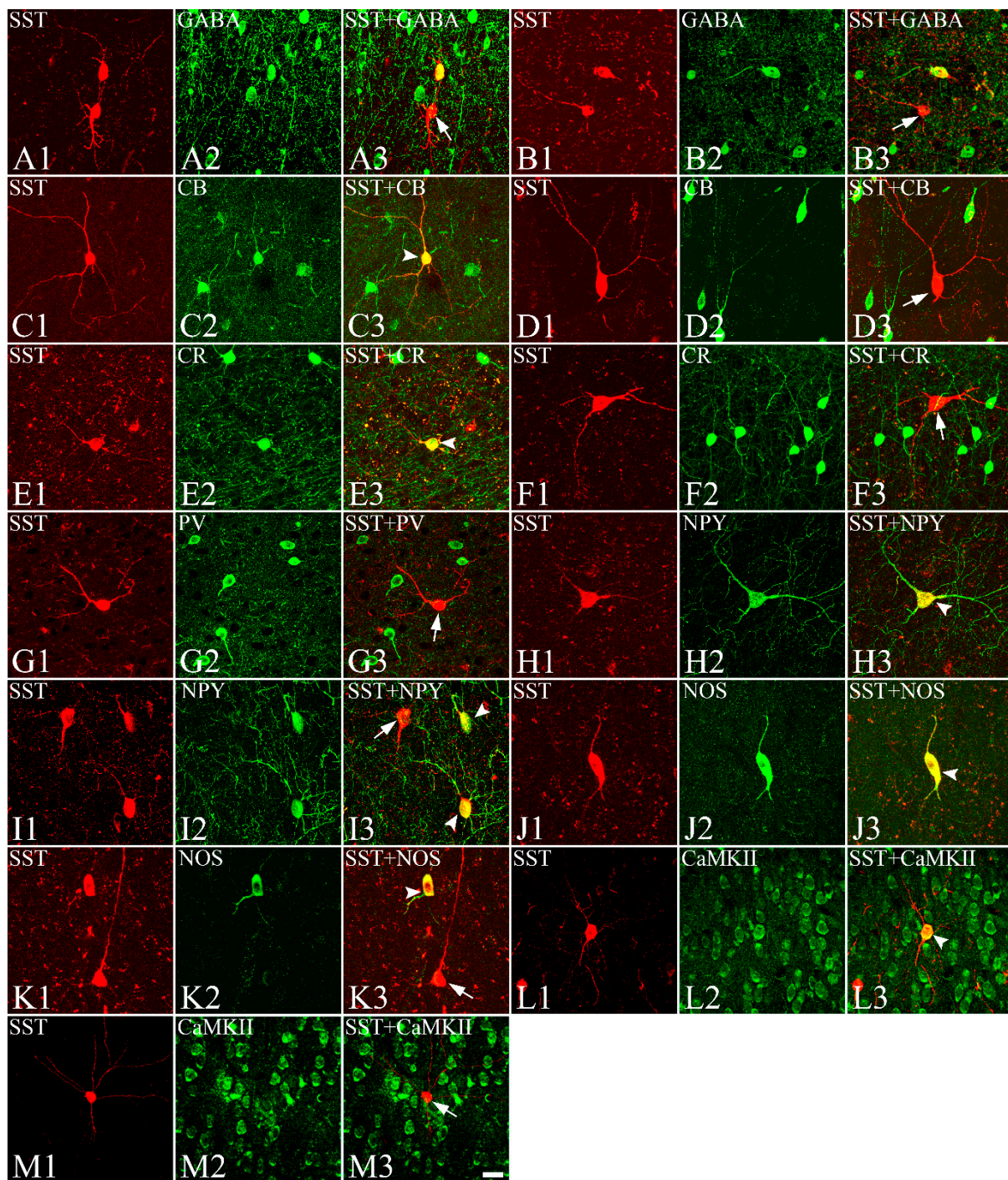
Figure 3. Fluorescence confocal photomicrographs of colocalization of SST neurons (**A1,B1,C1,D1, E1,F1,G1,H1,I1,J1,K1,L1,M1**) labeled with Cy3, shown in red, with GABA- (**A2,B2**), CB- (**C2,D2**), CR- (**E2,F2**), PV- (**G2**), NPY- (**H2,I2**), NOS- (**J2,K2**), or CaMKII-IR (**L2,M2**) neurons labeled with FITC, shown in green, and overlapped images of SST with GABA (**A3,B3**), CBPs (**C3,D3,E3,F3,G3**), NPY (**H3,I3**), NOS (**J3,K3**), and CaMKII (**L3,M3**) in the gerbil VC. Some of the SST neurons co-expressed GABA (arrowheads in **A3,B3**), CB (arrowhead in **C3**), CR (arrowhead in **E3**), NPY (arrowheads in **H3,I3**), NOS (arrowheads in **J3,K3**), or CaMKII (arrowhead in **L3**). However, none of the SST neurons co-expressed PV (arrow in **G3**). Single-labeled SST neurons were marked with arrows. SST, somatostatin; GABA, gamma-aminobutyric acid; CB, calbindin-D28K; CR, calretinin; PV, parvalbumin; NPY, neuropeptide Y; NOS, nitric oxide synthase; CaMKII, calcium/calmodulin-dependent protein kinase II. Scale bar = 20 μm.
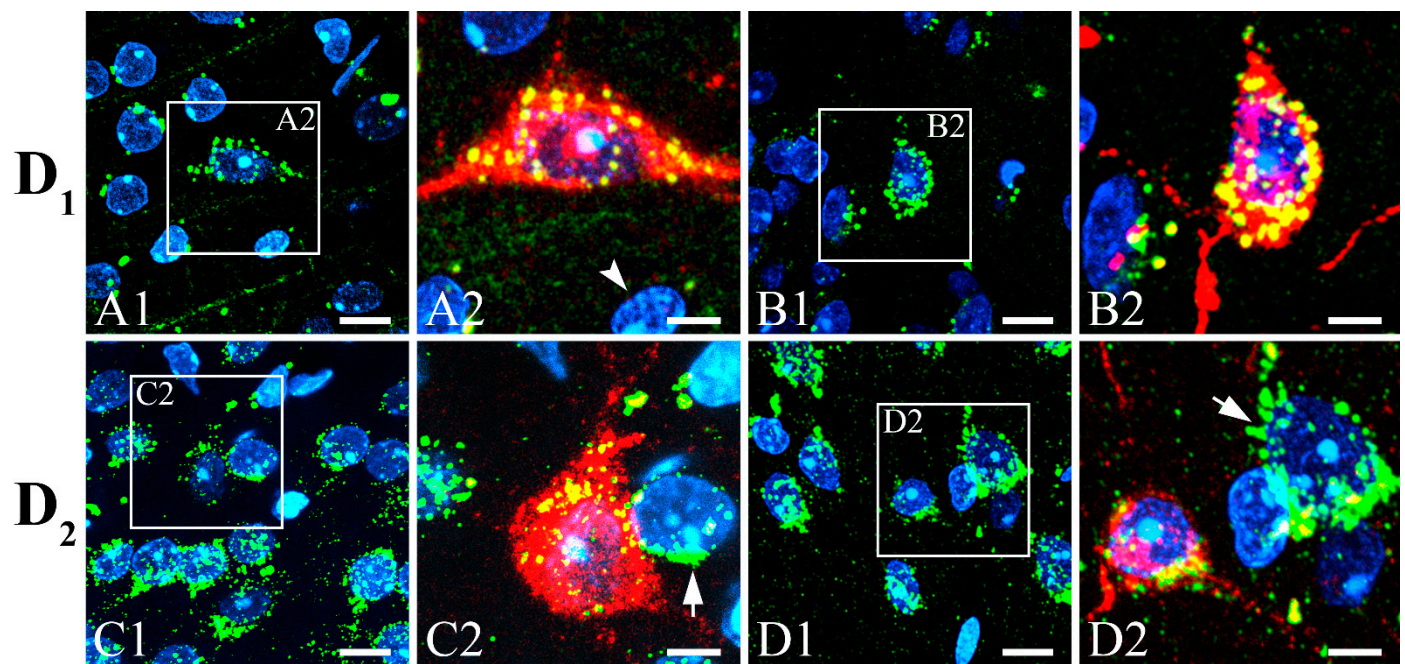
Figure 4. Double-labeling of SST with D_1 or D_2 dopamine receptors in gerbil VC. Fluorescence photomicrographs of immunostained D_1 (**A,B**) and D_2 (**C,D**) dopamine receptors (green) surround some cell nuclei stained with 4′,6-diamidino-2-phenylindole (DAPI) (blue). (**A2,B2,C2,D2**) Magnification of white boxes (**A1,B1,C1,D1**) showing merged images of cells co-expressing both SST (red) and dopamine receptors. SST neurons were clearly surrounded by immunopuncta of D_1 (**A2,B2**) and D_2 (**C2,D2**) dopamine receptors. There are cells surrounded by dopamine receptors without SST immunoreactivity (arrows). There are also cells that are immunoreactive to neither dopamine receptors nor SST (arrowhead). Scale bar = 10 (**A1–D1**) and 5 μm (**A2–D2**). D_1, D_1 dopamine receptor; D_2, D_2 dopamine receptor.

Table 2. Percentage of SST neurons, and neurons double-labeled with GABA, CBPs, NPY, NOS, or CaMKII in the gerbil VC.

Antibodies	Animal	No. Sections	No. SST Cells	No. Double	% Double (Mean $\pm$ S.D.)
GABA	#1	3	70	23	32.85 $\pm$ 5.59
	#2	3	73	23	31.50 $\pm$ 3.38
	#3	3	54	20	37.03 $\pm$ 6.75
GABA total		9	197	66	33.50 $\pm$ 6.04
CB	#1	3	78	19	24.35 $\pm$ 0.56
	#2	3	63	16	25.39 $\pm$ 1.55
	#3	3	72	16	22.22 $\pm$ 5.69
CB total		9	212	51	24.05 $\pm$ 3.73
CR	#1	3	58	9	15.51 $\pm$ 4.29
	#2	3	84	14	16.66 $\pm$ 0.56
	#3	3	97	17	17.52 $\pm$ 0.65
CR total		9	239	40	16.73 $\pm$ 2.77
PV	#1	3	67	0	0
	#2	3	65	0	0
	#3	3	61	0	0
PV total		9	193	0	0

Table 2. *Cont.*

Antibodies	Animal	No. Sections	No. SST Cells	No. Double	% Double (Mean $\pm$ S.D.)
NPY	#1	3	84	71	84.52 $\pm$ 3.73
	#2	3	103	73	70.87 $\pm$ 2.49
	#3	3	84	73	86.90 $\pm$ 3.47
NPY total		9	271	217	80.07 $\pm$ 7.80
NOS	#1	3	68	55	80.88 $\pm$ 2.40
	#2	3	103	73	67.20 $\pm$ 5.71
	#3	3	84	73	84.72 $\pm$ 5.42
NOS total		9	265	200	75.41 $\pm$ 8.64
CaMKII	#1	3	86	54	62.79 $\pm$ 8.53
	#2	3	85	50	58.82 $\pm$ 5.11
	#3	3	83	60	72.29 $\pm$ 6.03
CaMKII total		9	254	164	64.57 $\pm$ 8.77

GABA, gamma-aminobutyric acid; CB, calbindin-D28K; CR, calretinin; PV, parvalbumin; NPY, neuropeptide Y; NOS, nitric oxide synthase; CaMKII, calcium/calmodulin-dependent protein kinase II.
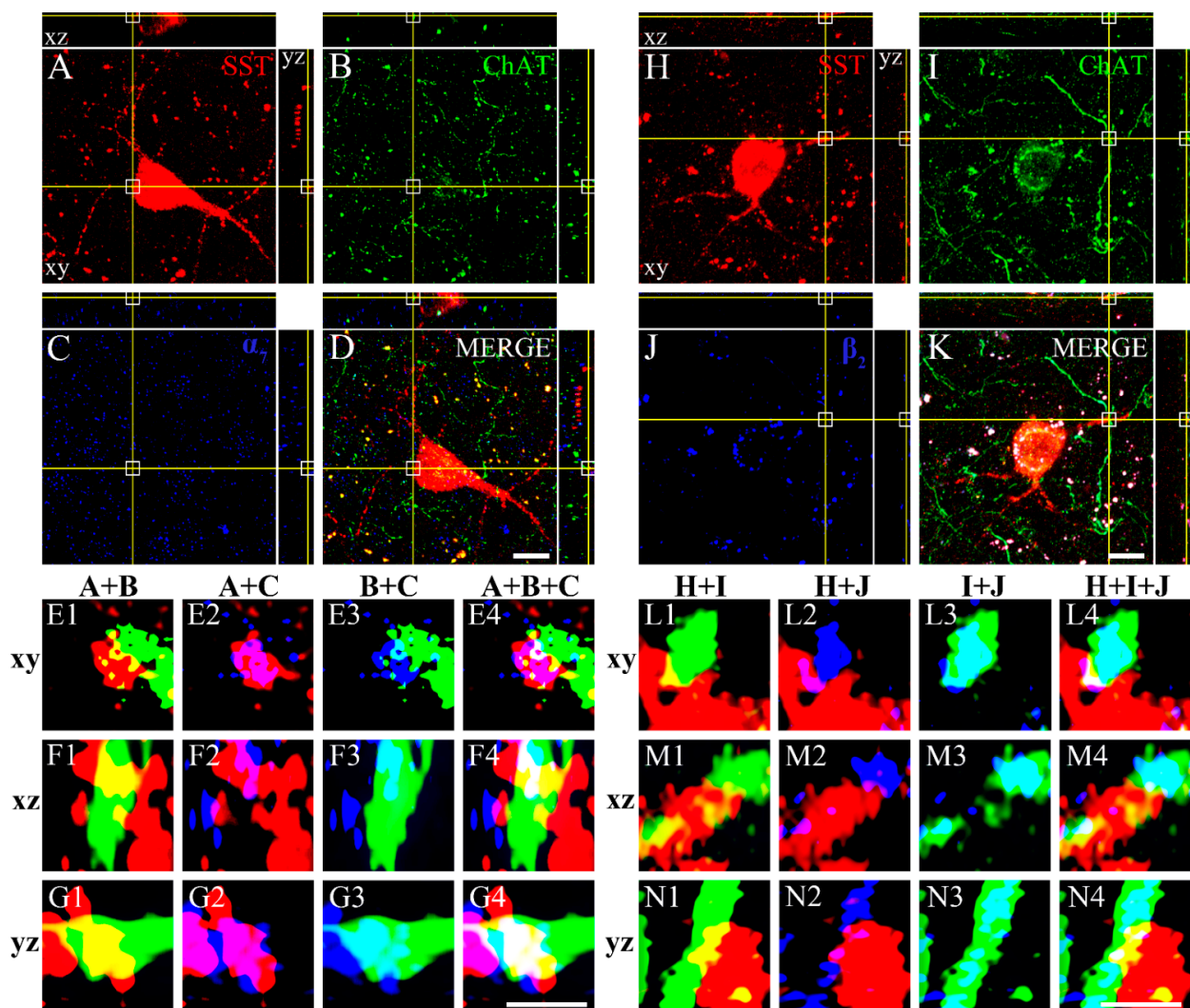

Figure 5. Triple-labeled fluorescence photomicrographs of SST neurons with ChAT-IR fibers and nAChRs. Orthogonal view of a confocal z-stack image of the SST neurons (red, **A,H**), ChAT-IR fibers

(green, **B**,**I**), α_7 nAChRs (blue, false color of infrared fluorescence, **C**), merged image of SST neurons with ChAT-IR fibers and α_7 nAChRs (**D**), β_2 nAChRs (blue, false color of infrared fluorescence, **J**), and merged image of SST neurons with ChAT-IR fibers and β_2 nAChRs (**K**). High-power images in crosshair from the xy (**E1**–**E4**), xz (**F1**–**F4**), and yz (**G1**–**G4**) planes from A–D, respectively. High-power images in crosshair from the xy (**L1**–**L4**), xz (**M1**–**M4**), and yz (**N1**–**N4**) planes from H to K, respectively. (**E1**,**F1**,**G1**) Merged images of SST neurons (**A**) and ChAT-IR fibers (**B**) in the xy, xz, and yz planes, respectively. (**E2**,**F2**,**G2**) Merged images of SST neurons and α_7 nAChRs immunopuncta in the xy, xz, and yz planes, respectively. (**E3**,**F3**,**G3**) Merged images of ChAT-IR fibers and α_7 nAChRs immunopuncta in the xy, xz, and yz planes, respectively. (**E4**,**F4**,**G4**) Merged images of SST neurons, ChAT-IR fibers, and α_7 nAChRs immunopuncta in the xy, xz, and yz planes, respectively. (**L1**,**M1**,**N1**) Merged images of SST neurons (**H**) and ChAT-IR fibers (**I**) in the xy, xz, and yz planes, respectively. (**L2**,**M2**,**N2**) Merged images of SST neurons and β_2 nAChRs immunopuncta in the xy, xz, and yz planes, respectively. (**L3**,**M3**,**N3**) Merged images of ChAT-IR fibers and β_2 nAChRs immunopuncta in the xy, xz, and yz planes, respectively. (**L4**,**M4**,**N4**) Merged images of SST neurons, ChAT-IR fibers, and β_2 nAChRs immunopuncta in the xy, xz, and yz planes, respectively. SST, somatostatin; ChAT, choline acetyltransferase; α_7, α_7 nicotinic acetylcholine receptor; β_2, β_2 nicotinic acetylcholine receptor. Scale bar = 10 (**A**–**D**,**H**–**K**) and 1 μm (**E1**–**G4**,**L1**–**N4**).

4. Discussion

The present study showed that SST neurons were mainly distributed in layer V of the Mongolian gerbil VC and showed various morphologies. Our results also showed diverse heterogenous types of SST neurons based on the expressional patterns of CBPs, NPY, and NOS. Some SST neurons appeared to be innervated by dopaminergic and cholinergic inputs.

The immunocytochemical labeling of SST neurons showed both intensely and weakly labeled cells. These two labeling patterns represent different distributional characteristics. Intensely labeled SST neurons were highly concentrated in the lower layers, V and VI, of VC. However, weakly labeled neurons were distributed throughout layers III and IV and with a peak at V. Both types of neurons showed almost no labeled cells in layer I. This is highly consistent with other reported animals [40–43]. Similarly to the present results, previous studies in rat [32,41] and cat [34] VC also showed the prominent distribution of SST neurons on infragranular layers. However, there are differences in distribution patterns among studies with various animals. The majority of SST neurons were in layer II and III in rat [40,42,43], mouse [14], rabbit [38], and monkey [32] VC. In addition, our results showed a relatively large portion of weakly labeled SST neurons in layer IV, which seems to be an unusual pattern compared to other studies, describing the presence of very few cells in layer IV of rat [39,41], cat [34], rabbit [38], and monkey VC [32]. Although there is still no explanation for the differences in distribution between species, these facts might suggest that there are subtle differences in the role of SST neurons in VC between animals.

The cortex contains extremely large numbers of functional and morphological types of neurons [27]. Based on the cortical tiling arguments, hundreds of different cell types have been suggested in the neocortex [28]. Moreover, based on the investigations of functional connectivity revealed by laser scanning photostimulation, at least 156 cell types have been suggested in layer IIIb in the primary VC of macaque monkeys [29]. The morphology of SST neurons in the gerbil VC showed diverse types of non-pyramidal interneurons. The majority of the cells were round/oval cells. The next most common were the stellate cells. Vertical fusiform and horizontal cells were also found in the gerbil VC. As in the present study, SST neurons in rat [39–41,46] and monkey VC [32] are non-pyramidal cells with a multipolar, bitufted morphology. The cat VC also contains the same morphological features of SST neurons with multipolar, bitufted, bipolar, and Martinotti cells [34,37]. However, in cats and rabbits, few pyramidal-like cells were observed [35,86]. Taken together, these results show that the morphological shape of SST neurons in VC is in general agreement among animal species. However, the various distinct types of SST neurons reflect the

diverse functions and connections with other neurons of SST neurons in VC. It will be very important to elucidate the functions and circuits of each type of SST neurons in the future.

SST neurons in the gerbil VC showed variable sizes but small-to-medium sized cells were most prevalent. No cells bigger than 15 μm were found. Similarly to the present study, the monkey VC also contained small multipolar SST neurons with diameters of 10 to 12 μm. However, contrary to the present study, large multipolar cells of more than 16 μm in diameter and bitufted cells with lengths of 18 to 30 μm have also been described in monkey VC [32]. Small round cell bodies, $8 \times 8 \ \mu m^2$ in size, and fusiform cell bodies, $20 \times 10 \ \mu m^2$ in size, have been reported in rat and monkey neocortices, including the VC [31]. Finally, SST neurons in the cat VC were medium-to-large sized (16–30 μm) cells [34,35]. Thus, the sizes of SST neurons between animals are generally inconsistent. The importance of this diversity in size is not yet obvious.

SST neurons are a major group of GABAergic neurons in mammalian cortical areas, including the VC [14]. In the present study, we found that approximately one-third of SST neurons contained GABA. This result is quite contradictory to the fact that SST neurons are thought to be almost GABAergic in VC [34,42]. However, there is a proportion of SST neurons that do not express GABA. Thus, some SST neurons (2–20%) were not labeled with GABA in rat VC [14,39]. In the hippocampus (9%) and entorhinal cortex (18%), various numbers of SST neurons were not labeled with GABA [87,88]. This discrepancy indicates the existence of species diversity and location dependence. Moreover, the presence of GABAergic neurons outside the boundary of interneurons in the mouse neocortex suggests the possibility that unconventional groups of SST neurons could exist [89].

The low rate of GABA expression in SST neurons raises the question of non-GABAergic neuron functions. The excitatory neuronal marker CaMKII was colocalized with many SST neurons in the present study. It is widely agreed that SST mainly acts as an inhibitory neurotransmitter or neuromodulator in the central nervous system. However, there have been reports of the excitatory effects of SST. For example, SST had a potent excitatory effect on the hippocampus [90], and the effects of SST on mammalian cortical neurons in culture were predominantly excitatory [91]. Most (>90%) SST neurons in the Pre-Bötzinger complex of rat medulla contained vesicular glutamate transporter 2 [92]. In the nucleus of the solitary tract of the rats, one-third of SST neurons, which do not express GAD-67, were found to be vesicular glutamate transporter positive [93]. An unpublished article by Cattaneo [94] suggested that striatal SST interneurons expressed mRNAs for both glutamate and GABA vesicular transporter. These results suggest that the actions of SST are both inhibitory and excitatory.

Many cortical interneurons selectively express specific CBPs [20]. In general, CR and PV are known to form non-overlapping populations with SST neurons and have distinct roles [5,95–97]. For example, SST neurons did not express CR in the rat VC [41]. However, the mouse VC expressed 34.3% of CR in SST neurons [97]. An overlapping population (30%) of SST neurons with CR-IR neurons across frontal, somatosensory, and VC has also been reported in mice [98]. Similarly, some SST neurons (16.73%) were double-labeled with CR in the gerbil VC. Our study showed distinct populations of SST neurons from PV, which is in agreement with many former studies. For example, none of the SST neurons colocalized with PV in the rat VC [41]. However, a small number (10%) of cells in the somatosensory cortex of rats co-expressed both PV and SST at the mRNA level [99]. CB is known to comprise a large portion of SST neurons in the cortex [41,95,96]. In the rat VC, 86.3% of SST neurons co-expressed CB [41], 85% of SST neurons co-expressed CB in layers II/III, and 92% in layers V and VI [95]. However, only one-fourth of SST neurons colocalized with CB in the gerbil VC. In the mouse cingulate cortex, one-third of SST neurons co-expressed CB in layers II/III [100]. The combined results again indicate the existence of diversity among animal species and subtle differences in roles that SST neuronal subtypes play.

NPY and NOS have been widely used as markers for the classification of neurochemically distinct interneurons in VC [84,85]. The present study shows large numbers of SST neurons co-expressing NPY (80.07%) and NOS (75.41%). Similarly, 97% and 98% of SST

neurons expressed NPY and NOS, respectively, in the guinea pig dorsal striatum [101]. In the rat striatum, 78.3% of SST neurons also expressed NPY [102]. However, only 1.7% of SST neurons expressed NOS in the rat VC [41], and 7% of SST neurons express NOS in the mouse hippocampus [103]. Again, the difference in the expression rates of NPY and NOS in SST neurons between animals and regions seems to be clear. However, the present and previous studies suggest that SST neurons can be further subdivided based on their respective abundance and scarcity of various CBPs, NPY, and NOS. These SST neurons subtypes can present diverse physiological relevance.

The dopamine system controls the physiological function of mood. Indeed, depression is characterized by a decreased dopamine level [104]. The level of SST is also closely related to mood symptoms, whereby decreased SST is a pathological feature in depression [105]. Dopamine receptors are distributed throughout the brain [78]. D_1 [106] and D_2 [107] dopamine receptors have been found in the VC. Previous studies have shown that a few SST neurons contained detectable D_1 dopamine receptor mRNA [108] and that dopamine affected the level of SST via D_1 and D_2 dopamine receptors in the striatum [109]. D_1 and D_2 receptors are present in inhibitory interneurons, including SST neurons in the monkey frontal eye field [110]. However, minimal colabeling between D_1 dopamine receptor and SST interneurons was shown in the mouse prefrontal cortex [111]. The present study showed the positioning of D_1 and D_2 dopamine receptors in SST neurons in the gerbil VC. These results may suggest a neural connection of dopaminergic neurons to the SST neurons in the VC. Previous studies have shown that SST neurons are responsible for the surround suppression of pyramidal cells in VC [112] and can improve the cognitive function of visual perception in the VC via the inhibition of excitatory neurons to PV+ inhibitory neurons [8,113]. Many previous studies have shown that ChAT plays an important modulatory function in cognition and memory through nAChRs. Additionally, various subtypes of nAChRs have been found in the cerebral cortex [114]. SST is also involved in neuroplasticity, such as enhanced ocular dominance plasticity in VC. Furthermore, SST neurons were activated by acetylcholine [115] and nicotinic receptors [4]. The cholinergic facilitation of the lateral inhibition of neighboring pyramidal neurons in the mouse neocortex is mediated by the activation of β_2 subunit-containing nAChRs that depolarize SST-positive Martinotti cells [116]. The nAChR modulator, the Lynx family, has been found in SST interneurons in the mouse VC [117]. In this study, we found the presence of α_7 and β_2 subtypes of nAChRs in the SST neurons. These results suggest an acetylcholine-SST circuit in the VC, and such information will significantly improve our understanding of SST neuron circuits.

There are differences in the organization of the area of VC between diurnal and nocturnal rodents. The percentage of the cortex devoted to area 17 is significantly greater in the diurnal Nile grass rat compared to the nocturnal Norway rat [118]. However, there were no clear cellular composition differences in area 17 between nocturnal and diurnal rats [118]. The squirrel, a highly visual diurnal rodent with a cone-dominated retina, has a larger amount of cortex devoted to VC compared to nocturnal rodents [119]. The connections from the lateral geniculate nucleus to the VC shows that the squirrel has a well-developed retino-geniculo-cortical system compared to that of the laboratory rat [120]. Several response properties of neurons in the squirrel V1 set diurnal squirrels apart from nocturnal rodents. For example, the squirrel has laminar specificity for direction selectivity, which is lacking in nocturnal rats and mice and has fewer orientation-selective cells in V1 than nocturnal mammals [121]. The V1 of the squirrel contains cells that are tuned to high temporal frequencies, reflecting cone-based vision [121]. Thus, the diurnal squirrel V1 has many similar response properties to larger mammals with a well-developed visual system [122]. However, similarly to other less visual rodents, structured functional maps in visual systems, such as columnar organizations or orientation maps, were lacking in the V1, even in more visual diurnal rodents, such as squirrels [123]. Recently, the orientation- and direction-selective neurons and their spatial layout have been characterized in the primary VC of the large diurnal rodent agoutis. Neurons exhibited orientation and direction

preferences in agoutis, with a bias for horizontal contours [124]. The aggregate classical receptive field of agoutis was similar to that of cat areas 17 and 18 and was smaller than that of nocturnal rats and mice [124]. However, the response properties, such as orientation and direction selectivity, simple and complex cells, and spatial and temporal tuning, that have been fairly well-documented in diurnal squirrels, have not yet been well-studied in gerbils. Future studies should elucidate these response properties in gerbils to better understand the diurnal gerbil visual system and the diverse functional organization of the rodent VC as cortical functional architecture can vary greatly from species to species [118,123,124].

Studies on the localization of SST in the human brain have been somewhat limited. One study, using immunocytochemistry, found widespread SST neurons with varying morphologies, sizes, and fibers in whole brain regions and forebrain areas [125]. Distinct topographical localizations of two SST receptor (SSTR) subpopulations in the human cortex have been described using radioligands [126]. The $SSTR_1$ was preferentially localized in layers V and VI, while $SSTR_2$ was concentrated in the superficial cortical layers (I–IV) and particularly enriched in parts of the lamina IV. The $SSTR_4$ localization in the human brain has also been found to include the VC [127]. Both cell bodies and fibers existed at layers III–VI—abundant in layer III—and cell bodies were lacking in I–II. SST mRNA-containing neurons were widely distributed in several areas of the human brain, including the VC [128]. Neurons containing SSTR mRNA also localized in the human cortex, which identified the noticeable distribution of $SSTR_3$ mRNA in layers IVc and V of the VC [129]. In the human neocortex, it has been found that the depolarization of SST-positive Martinotti cells by acetylcholine mediates the cholinergic facilitation of lateral inhibition [116]. These results strongly support the evidence that SST neurons exist in the human VC. However, there have been no detailed studies on cell morphology, laminar distribution, or neural networks of SST neurons in the human VC comparable with the present result. Studies in animals are often closely related to humans, but in-depth research on the human VC will be essential for a clear understanding of the organization and function of SST neurons in humans.

The dysfunction of SST in the brain is closely linked to various human neuropsychiatric and neurodegenerative disorders. Patients with major depressive disorder show decreased SST levels [12]. Other neuropsychiatric disorders, such as schizophrenia and bipolar disorder, showed a reduction in SST gene expression and fewer SST-expressing neurons in various brain areas [11,130]. Neurodegenerative disorders, such as Alzheimer's and Parkinson's disease, are also closely linked to reduced levels of SST in cortical and subcortical regions [6,80]. Many aspects of the anatomical, physiological, pharmacological, and genetic characteristics of SST neurons remain unknown. However, the attribution of SST in the control of various human brain diseases demands in-depth information, such as specific laminar distribution, distinct cell types, and specific cortical wiring patterns of SST neurons.

5. Conclusions

SST neurons included a highly diverse group of interneurons both morphologically and with respect to the presence and absence of GABA, CB, CR, PV, NPY, NOS, and CaMKII implying diverse functional roles. The present study suggests that SST neurons in the VC receive inputs from dopamine and acetylcholine at least via D_1 and D_2 dopamine receptors and α_7 and β_2 nAChRs for wiring of VC. It will be essential to compare the present study with molecular, physiological, pharmacological, and genetic levels to enhance the understanding of SST function in the VC. With this knowledge, links can be made between SST function and SST-related neurological disorders in humans.

Author Contributions: Conceptualization, C.-J.J.; Methodology, K.-M.K., M.-J.L. and C.-J.J.; Software, M.-J.L.; Validation, K.-M.K., M.-J.L., H.-S.C. and C.-J.J.; Formal Analysis, K.-M.K. and M.-J.L.; Investigation, K.-M.K., M.-J.L., H.-S.C. and C.-J.J.; Resources, C.-J.J.; Data Curation, K.-M.K. and M.-J.L.; Writing—Original Draft Preparation, M.-J.L.; Writing—Review and Editing, K.-M.K., M.-J.L., H.-S.C. and C.-J.J.; Visualization, K.-M.K. and M.-J.L.; Supervision, J.-H.P. and C.-J.J.; Project Administration,

J.-H.P. and C.-J.J.; Funding Acquisition, J.-H.P. and C.-J.J. All authors have read and agreed to the published version of the manuscript.

Institutional Review Board Statement: The study was conducted according to the guidelines of the Declaration of Helsinki, and approved by the Animal Care and Use Committee of Kyungpook National University (permission NO. 2014-0181).

Informed Consent Statement: Not applicable.

Data Availability Statement: Any additional data will be available upon request to the corresponding author.

Conflicts of Interest: The authors declare no conflict of interest. The funders had no role in the design of the study; in the collection, analyses, or interpretation of data; in the writing of the manuscript, or in the decision to publish the results.

References

1. Brazeau, P.; Vale, W.; Burgus, R.; Ling, N.; Butcher, M.; Rivier, J.; Guillemin, R. Hypothalamic polypeptide that inhibits the secretion of immunoreactive pituitary growth hormone. *Science* **1973**, *179*, 77–79. [CrossRef]
2. Strowski, M.Z.; Blake, A.D. Function and expression of somatostatin receptors of the endocrine pancreas. *Mol. Cell. Endocrinol.* **2008**, *286*, 169–179. [CrossRef]
3. Piqueras, L.; Martínez, V. Role of somatostatin receptors on gastric acid secretion in wild-type and somatostatin receptor type 2 knockout mice. *Naunyn-Schmiedebergs Arch. Pharmacol.* **2004**, *370*, 510–520. [CrossRef]
4. Liguz-Lecznar, M.; Urban-Ciecko, J.; Kossut, M. Somatostatin and Somatostatin-Containing Neurons in Shaping Neuronal Activity and Plasticity. *Front. Neural Circuits* **2016**, *10*, 48. [CrossRef] [PubMed]
5. Khan, A.G.; Poort, J.; Chadwick, A.; Blot, A.; Sahani, M.; Mrsic-Flogel, T.D.; Hofer, S.B. Distinct learning-induced changes in stimulus selectivity and interactions of GABAergic interneuron classes in visual cortex. *Nat. Neurosci.* **2018**, *21*, 851–859. [CrossRef] [PubMed]
6. Honoré, E.; Khlaifia, A.; Bosson, A.; Lacaille, J.C. Hippocampal Somatostatin Interneurons, Long-Term Synaptic Plasticity and Memory. *Front. Neural Circuits* **2021**, *15*, 687558. [CrossRef]
7. Adler, A.; Zhao, R.; Shin, M.E.; Yasuda, R.; Gan, W.B. Somatostatin-Expressing Interneurons Enable and Maintain Learning-Dependent Sequential Activation of Pyramidal Neurons. *Neuron* **2019**, *102*, 202–216.e207. [CrossRef]
8. Song, Y.H.; Hwang, Y.S.; Kim, K.; Lee, H.R.; Kim, J.H.; Maclachlan, C.; Dubois, A.; Jung, M.W.; Petersen, C.C.H.; Knott, G.; et al. Somatostatin enhances visual processing and perception by suppressing excitatory inputs to parvalbumin-positive interneurons in V1. *Sci. Adv.* **2020**, *6*, eaaz0517. [CrossRef] [PubMed]
9. Keller, A.J.; Dipoppa, M.; Roth, M.M.; Caudill, M.S.; Ingrosso, A.; Miller, K.D.; Scanziani, M. A Disinhibitory Circuit for Contextual Modulation in Primary Visual Cortex. *Neuron* **2020**, *108*, 1181–1193.e1188. [CrossRef]
10. Huang, P.; Xiang, X.; Chen, X.; Li, H. Somatostatin Neurons Govern Theta Oscillations Induced by Salient Visual Signals. *Cell Rep.* **2020**, *33*, 108415. [CrossRef]
11. Hashimoto, T.; Bazmi, H.H.; Mirnics, K.; Wu, Q.; Sampson, A.R.; Lewis, D.A. Conserved regional patterns of GABA-related transcript expression in the neocortex of subjects with schizophrenia. *Am. J. Psychiat.* **2008**, *165*, 479–489. [CrossRef]
12. Fee, C.; Banasr, M.; Sibille, E. Somatostatin-Positive Gamma-Aminobutyric Acid Interneuron Deficits in Depression: Cortical Microcircuit and Therapeutic Perspectives. *Biol. Psychiatry* **2017**, *82*, 549–559. [CrossRef] [PubMed]
13. Kumar, U.; Singh, S. Role of Somatostatin in the Regulation of Central and Peripheral Factors of Satiety and Obesity. *Int. J. Mol. Sci.* **2020**, *21*, 2568. [CrossRef]
14. Gonchar, Y.; Wang, Q.; Burkhalter, A. Multiple distinct subtypes of GABAergic neurons in mouse visual cortex identified by triple immunostaining. *Front. Neuroanat.* **2007**, *1*, 3. [CrossRef]
15. Rudy, B.; Fishell, G.; Lee, S.; Hjerling-Leffler, J. Three groups of interneurons account for nearly 100% of neocortical GABAergic neurons. *Dev. Neurobiol.* **2011**, *71*, 45–61. [CrossRef] [PubMed]
16. Tremblay, R.; Lee, S.; Rudy, B. GABAergic Interneurons in the Neocortex: From Cellular Properties to Circuits. *Neuron* **2016**, *91*, 260–292. [CrossRef]
17. Wamsley, B.; Fishell, G. Genetic and activity-dependent mechanisms underlying interneuron diversity. *Nat. Rev. Neurosci.* **2017**, *18*, 299–309. [CrossRef]
18. Markram, H.; Toledo-Rodriguez, M.; Wang, Y.; Gupta, A.; Silberberg, G.; Wu, C. Interneurons of the neocortical inhibitory system. *Nat. Rev. Neurosci.* **2004**, *5*, 793–807. [CrossRef] [PubMed]
19. Elíes, J.; Yáñez, M.; Pereira, T.M.C.; Gil-Longo, J.; MacDougall, D.A.; Campos-Toimil, M. An Update to Calcium Binding Proteins. *Adv. Exp. Med. Biol.* **2020**, *1131*, 183–213. [CrossRef]

20. Baimbridge, K.G.; Celio, M.R.; Rogers, J.H. Calcium-binding proteins in the nervous system. *Trends Neurosci.* **1992**, *15*, 303–308. [CrossRef]
21. Sohn, J.; Hioki, H.; Okamoto, S.; Kaneko, T. Preprodynorphin-expressing neurons constitute a large subgroup of somatostatin-expressing GABAergic interneurons in the mouse neocortex. *J. Comp. Neurol.* **2014**, *522*, 1506–1526. [CrossRef]
22. Yavorska, I.; Wehr, M. Somatostatin-Expressing Inhibitory Interneurons in Cortical Circuits. *Front. Neural Circuits* **2016**, *10*, 76. [CrossRef]
23. Karagiannis, A.; Gallopin, T.; Dávid, C.; Battaglia, D.; Geoffroy, H.; Rossier, J.; Hillman, E.M.; Staiger, J.F.; Cauli, B. Classification of NPY-expressing neocortical interneurons. *J. Neurosci.* **2009**, *29*, 3642–3659. [CrossRef]
24. Allen, J.M.; Bloom, S.R. Neuropeptide Y: A putative neurotransmitter. *Neurochem. Int.* **1986**, *8*, 1–8. [CrossRef]
25. Jaglin, X.H.; Hjerling-Leffler, J.; Fishell, G.; Batista-Brito, R. The origin of neocortical nitric oxide synthase-expressing inhibitory neurons. *Front. Neural Circuits* **2012**, *6*, 44. [CrossRef]
26. Niell, C.M. Cell types, circuits, and receptive fields in the mouse visual cortex. *Annu. Rev. Neurosci.* **2015**, *38*, 413–431. [CrossRef] [PubMed]
27. Masland, R.H. Neuronal cell types. *Curr. Biol.* **2004**, *14*, R497–R500. [CrossRef] [PubMed]
28. Stevens, C.F. Neuronal diversity: Too many cell types for comfort? *Curr. Biol.* **1998**, *8*, R708–R710. [CrossRef]
29. Sawatari, A.; Callaway, E.M. Diversity and cell type specificity of local excitatory connections to neurons in layer 3B of monkey primary visual cortex. *Neuron* **2000**, *25*, 459–471. [CrossRef]
30. Scala, F.; Kobak, D.; Shan, S.; Bernaerts, Y.; Laturnus, S.; Cadwell, C.R.; Hartmanis, L.; Froudarakis, E.; Castro, J.R.; Tan, Z.H.; et al. Layer 4 of mouse neocortex differs in cell types and circuit organization between sensory areas. *Nat. Commun.* **2019**, *10*, 4174. [CrossRef]
31. Hendry, S.H.; Jones, E.G.; Emson, P.C. Morphology, distribution, and synaptic relations of somatostatin- and neuropeptide Y-immunoreactive neurons in rat and monkey neocortex. *J. Neurosci.* **1984**, *4*, 2497–2517. [CrossRef]
32. Campbell, M.J.; Lewis, D.A.; Benoit, R.; Morrison, J.H. Regional heterogeneity in the distribution of somatostatin-28- and somatostatin-28(1-12)-immunoreactive profiles in monkey neocortex. *J. Neurosci.* **1987**, *7*, 1133–1144. [CrossRef]
33. Demeulemeester, H.; Arckens, L.; Vandesande, F.; Orban, G.A.; Heizmann, C.W.; Pochet, R. Calcium binding proteins and neuropeptides as molecular markers of GABAergic interneurons in the cat visual cortex. *Exp. Brain Res.* **1991**, *84*, 538–544. [CrossRef]
34. Demeulemeester, H.; Vandesande, F.; Orban, G.A.; Brandon, C.; Vanderhaeghen, J.J. Heterogeneity of GABAergic cells in cat visual cortex. *J. Neurosci.* **1988**, *8*, 988–1000. [CrossRef]
35. Demeulemeester, H.; Vandesande, F.; Orban, G.A. Immunocytochemical localization of somatostatin and cholecystokinin in the cat visual cortex. *Brain Res.* **1985**, *332*, 361–364. [CrossRef]
36. Somogyi, P.; Hodgson, A.J.; Smith, A.D.; Nunzi, M.G.; Gorio, A.; Wu, J.Y. Different populations of GABAergic neurons in the visual cortex and hippocampus of cat contain somatostatin- or cholecystokinin-immunoreactive material. *J. Neurosci.* **1984**, *4*, 2590–2603. [CrossRef] [PubMed]
37. Wahle, P. Differential regulation of substance P and somatostatin in Martinotti cells of the developing cat visual cortex. *J. Comp. Neurol.* **1993**, *329*, 519–538. [CrossRef] [PubMed]
38. Ramón, Y.; Cajal-Agüeras, S.; Contamina, P.; Parra, P.; Martinez-Millán, L.; De Carlos, J.A.; Ramo, C. The distribution of somatostatin-immunoreactive neurons in the visual cortex of adult rabbits and during postnatal development. *Brain Res.* **1985**, *359*, 379–382. [CrossRef]
39. Lin, C.S.; Lu, S.M.; Schmechel, D.E. Glutamic acid decarboxylase and somatostatin immunoreactivities in rat visual cortex. *J. Comp. Neurol.* **1986**, *244*, 369–383. [CrossRef] [PubMed]
40. McDonald, J.K.; Parnavelas, J.G.; Karamanlidis, A.N.; Brecha, N.; Koenig, J.I. The morphology and distribution of peptide-containing neurons in the adult and developing visual cortex of the rat. I. Somatostatin. *J. Neurocytol.* **1982**, *11*, 809–824. [CrossRef] [PubMed]
41. Gonchar, Y.; Burkhalter, A. Three distinct families of GABAergic neurons in rat visual cortex. *Cereb. Cortex* **1997**, *7*, 347–358. [CrossRef] [PubMed]
42. Papadopoulos, G.C.; Parnavelas, J.G.; Cavanagh, M.E. Extensive co-existence of neuropeptides in the rat visual cortex. *Brain Res.* **1987**, *420*, 95–99. [CrossRef]
43. Eadie, L.A.; Parnavelas, J.G.; Franke, E. Development of the ultrastructural features of somatostatin-immunoreactive neurons in the rat visual cortex. *J. Neurocytol.* **1987**, *16*, 445–459. [CrossRef] [PubMed]
44. Shimizu, T.; Karten, H.J. Immunohistochemical analysis of the visual wulst of the pigeon (*Columba livia*). *J. Comp. Neurol.* **1990**, *300*, 346–369. [CrossRef]
45. Feldman, S.C. Distribution of immunoreactive somatostatin (ISRIF) in the nervous system of the squid, Loligo pealei. *J. Comp. Neurol.* **1986**, *245*, 238–257. [CrossRef] [PubMed]
46. Paspalas, C.D.; Papadopoulos, G.C. Noradrenergic innervation of peptidergic interneurons in the rat visual cortex. *Cereb. Cortex* **1999**, *9*, 844–853. [CrossRef]
47. Schmechel, D.E.; Vickrey, B.G.; Fitzpatrick, D.; Elde, R.P. GABAergic neurons of mammalian cerebral cortex: Widespread subclass defined by somatostatin content. *Neurosci. Lett.* **1984**, *47*, 227–232. [CrossRef]
48. Cheal, M.L. The gerbil: A unique model for research on aging. *Exp. Aging Res.* **1986**, *12*, 3–21. [CrossRef]

49. Albers, H.J.; Gordon, S. Comparison of serum cholesterol esters in gerbil and rat. *Proc. Soc. Exp. Biol. Med.* **1962**, *109*, 860–863. [CrossRef]
50. Robinson, P.F. Metabolism of the Gerbil, *Meriones unguiculatus*. *Science* **1959**, *130*, 502–503. [CrossRef]
51. Gordon, S.; Cekleniak, W.P.; Stolzenberg, S.J.; Benitz, K.F.; Moraski, R.M. Biochemical and morphologic effects of cholesterol and its methyl ether in the gerbil. *Toxicol. Appl. Pharmacol.* **1961**, *3*, 315–334. [CrossRef]
52. Roscoe, H.G.; Fahrenbach, M.J. Cholesterol metabolism in the gerbil. *Proc. Soc. Exp. Biol. Med.* **1962**, *110*, 51–55. [CrossRef]
53. Gordon, S.; Stolzenberg, S.J.; Cekleniak, W.P. Effects of cholesterol and beta-sitosterol in the gerbil. *Am. J. Physiol.* **1959**, *197*, 671–673. [CrossRef]
54. Gordon, S.; Cekleniak, W.P. Serum lipoprotein pattern of the hypercholesteremic gerbil. *Am. J. Physiol.* **1961**, *201*, 27–28. [CrossRef] [PubMed]
55. Harrison, M.J.; Brownbill, D.; Lewis, P.D.; Russell, R.W. Cerebral edema following carotid artery ligation in the gerbil. *Arch. Neurol.* **1973**, *28*, 389–391. [CrossRef] [PubMed]
56. Jones-Mumby, C.J.; Axelsson, A. The vascular anatomy of the gerbil cochlea. *Am. J. Otolaryngol.* **1984**, *5*, 127–137. [CrossRef]
57. Peckova, R.; Sak, B.; Kvetonova, D.; Kvac, M.; Koritakova, E.; Foitova, I. The course of experimental giardiasis in Mongolian gerbil. *Parasitol. Res.* **2018**, *117*, 2437–2443. [CrossRef] [PubMed]
58. Belosevic, M.; Faubert, G.M.; MacLean, J.D.; Law, C.; Croll, N.A. Giardia lamblia infections in Mongolian gerbils: An animal model. *J. Infect. Dis.* **1983**, *147*, 222–226. [CrossRef] [PubMed]
59. Keplinger, S.; Beiderbeck, B.; Michalakis, S.; Biel, M.; Grothe, B.; Kunz, L. Optogenetic Control of Neural Circuits in the Mongolian Gerbil. *Front. Cell. Neurosci.* **2018**, *12*, 111. [CrossRef]
60. Lee, T.K.; Chen, B.H.; Lee, J.C.; Shin, M.C.; Cho, J.H.; Lee, H.A.; Choi, J.H.; Hwang, I.K.; Kang, I.J.; Ahn, J.H.; et al. Agedependent decreases in insulinlike growth factorI and its receptor expressions in the gerbil olfactory bulb. *Mol. Med. Rep.* **2018**, *17*, 8161–8166. [CrossRef]
61. Depner, M.; Tziridis, K.; Hess, A.; Schulze, H. Sensory cortex lesion triggers compensatory neuronal plasticity. *BMC. Neurosci.* **2014**, *15*, 57. [CrossRef]
62. Thomas, H.; Tillein, J.; Heil, P.; Scheich, H. Functional organization of auditory cortex in the mongolian gerbil (*Meriones unguiculatus*). I. Electrophysiological mapping of frequency representation and distinction of fields. *Eur. J. Neurosci.* **1993**, *5*, 882–897. [CrossRef]
63. Henschke, J.U.; Oelschlegel, A.M.; Angenstein, F.; Ohl, F.W.; Goldschmidt, J.; Kanold, P.O.; Budinger, E. Early sensory experience influences the development of multisensory thalamocortical and intracortical connections of primary sensory cortices. *Brain Struct. Funct.* **2018**, *223*, 1165–1190. [CrossRef]
64. Bertorelli, R.; Adami, M.; Ongini, E. The Mongolian gerbil in experimental epilepsy. *Ital. J. Neurol. Sci.* **1995**, *16*, 101–106. [CrossRef]
65. Levine, S.; Payan, H. Effects of ischemia and other procedures on the brain and retina of the gerbil (*Meriones unguiculatus*). *Exp. Neurol.* **1966**, *16*, 255–262. [CrossRef]
66. Kitabatake, T.T.; Marini, L.C.; Goncalves, R.B.; Bertolino, G.; de Souza, H.C.D.; de Araujo, J.E. Behavioral effects and neural changes induced by continuous and not continuous treadmill training, post bilateral cerebral ischemia in gerbils. *Behav. Brain Res.* **2015**, *291*, 20–25. [CrossRef] [PubMed]
67. Thiessen, D.D.; Goar, S. Stereotaxic atlas of the hypothalamus of the Mongolian gerbil (*Meriones unguiculatus*). *J. Comp. Neurol.* **1970**, *140*, 123–127. [CrossRef] [PubMed]
68. Radtke-Schuller, S.; Schuller, G.; Angenstein, F.; Grosser, O.S.; Goldschmidt, J.; Budinger, E. Brain atlas of the Mongolian gerbil (*Meriones unguiculatus*) in CT/MRI-aided stereotaxic coordinates. *Brain Struct. Funct.* **2016**, *221* (Suppl. 1), 1–272. [CrossRef]
69. Mankin, E.A.; Thurley, K.; Chenani, A.; Haas, O.V.; Debs, L.; Henke, J.; Galinato, M.; Leutgeb, J.K.; Leutgeb, S.; Leibold, C. The hippocampal code for space in Mongolian gerbils. *Hippocampus* **2019**, *29*, 787–801. [CrossRef] [PubMed]
70. Reme, C.E.; Wirz-Justice, A.; Terman, M. The visual input stage of the mammalian circadian pacemaking system: I. Is there a clock in the mammalian eye? *J. Biol. Rhythms* **1991**, *6*, 5–29. [CrossRef] [PubMed]
71. Govardovskii, V.I.; Rohlich, P.; Szel, A.; Khokhlova, T.V. Cones in the retina of the Mongolian gerbil, *Meriones unguiculatus*: An immunocytochemical and electrophysiological study. *Vision Res.* **1992**, *32*, 19–27. [CrossRef]
72. Bytyqi, A.H.; Layer, P.G. Lamina formation in the Mongolian gerbil retina (*Meriones unguiculatus*). *Anat. Embryol.* **2005**, *209*, 217–225. [CrossRef] [PubMed]
73. Baker, A.G.; Emerson, V.F. Grating acuity of the Mongolian gerbil (*Meriones unguiculatus*). *Behav. Brain Res.* **1983**, *8*, 195–209. [CrossRef]
74. Huber, G.; Heynen, S.; Imsand, C.; vom Hagen, F.; Muehlfriedel, R.; Tanimoto, N.; Feng, Y.; Hammes, H.P.; Grimm, C.; Peichl, L.; et al. Novel rodent models for macular research. *PLoS ONE* **2010**, *5*, e13403. [CrossRef] [PubMed]
75. Jeong, M.J.; Jeon, C.J. Localization of melanopsin-immunoreactive cells in the Mongolian gerbil retina. *Neurosci. Res.* **2015**, *100*, 6–16. [CrossRef]
76. Yang, S.; Luo, X.; Xiong, G.; So, K.F.; Yang, H.; Xu, Y. The electroretinogram of Mongolian gerbil (*Meriones unguiculatus*): Comparison to mouse. *Neurosci. Lett.* **2015**, *589*, 7–12. [CrossRef]

77. Macharadze, T.; Budinger, E.; Brosch, M.; Scheich, H.; Ohl, F.W.; Henschke, J.U. Early Sensory Loss Alters the Dendritic Branching and Spine Density of Supragranular Pyramidal Neurons in Rodent Primary Sensory Cortices. *Front. Neural Circuits* **2019**, *13*, 61. [CrossRef]

78. Beaulieu, J.M.; Gainetdinov, R.R. The physiology, signaling, and pharmacology of dopamine receptors. *Pharmacol. Rev.* **2011**, *63*, 182–217. [CrossRef]

79. Belujon, P.; Grace, A.A. Dopamine System Dysregulation in Major Depressive Disorders. *Int. J. Neuropsychopharmacol.* **2017**, *20*, 1036–1046. [CrossRef]

80. Lin, L.C.; Sibille, E. Reduced brain somatostatin in mood disorders: A common pathophysiological substrate and drug target? *Front. Pharmacol.* **2013**, *4*, 110. [CrossRef]

81. Koukouli, F.; Changeux, J.P. Do Nicotinic Receptors Modulate High-Order Cognitive Processing? *Trends Neurosci.* **2020**, *43*, 550–564. [CrossRef]

82. Hasselmo, M.E. The role of acetylcholine in learning and memory. *Curr. Opin. Neurobiol.* **2006**, *16*, 710–715. [CrossRef]

83. Hong, S.K.; Kim, J.Y.; Jeon, C.J. Immunocytochemical localization of calretinin in the superficial layers of the cat superior colliculus. *Neurosci. Res.* **2002**, *44*, 325–335. [CrossRef]

84. Lee, J.E.; Ahn, C.H.; Lee, J.Y.; Chung, E.S.; Jeon, C.J. Nitric oxide synthase and calcium-binding protein-containing neurons in the hamster visual cortex. *Mol. Cells.* **2004**, *18*, 30–39. [CrossRef]

85. Lee, M.J.; Lee, W.T.; Jeon, C.J. Organization of Neuropeptide Y-Immunoreactive Cells in the Mongolian gerbil (*Meriones unguiculatus*) Visual Cortex. *Cells* **2021**, *10*, 311. [CrossRef]

86. López-Mascaraque, L.; Ramo, C.; Contamina-Gonzalvo, P.; de Carlos, J. Layers I and VI of the visual cortex in the rabbit. A correlated Golgi and immunocytochemical study of somatostatin and vasoactive intestinal peptide containing neurons. *J. Brain Res.-J. Hirnforsch.* **1989**, *30*, 163–173.

87. Kosaka, T.; Wu, J.Y.; Benoit, R. GABAergic neurons containing somatostatin-like immunoreactivity in the rat hippocampus and dentate gyrus. *Exp. Brain Res.* **1988**, *71*, 388–398. [CrossRef] [PubMed]

88. Wouterlood, F.G.; Pothuizen, H. Sparse colocalization of somatostatin- and GABA-immunoreactivity in the entorhinal cortex of the rat. *Hippocampus* **2000**, *10*, 77–86. [CrossRef]

89. Tomioka, R.; Okamoto, K.; Furuta, T.; Fujiyama, F.; Iwasato, T.; Yanagawa, Y.; Obata, K.; Kaneko, T.; Tamamaki, N. Demonstration of long-range GABAergic connections distributed throughout the mouse neocortex. *Eur. J. Neurosci.* **2005**, *21*, 1587–1600. [CrossRef]

90. Dodd, J.; Kelly, J.S. Is somatostatin an excitatory transmitter in the hippocampus? *Nature* **1978**, *273*, 674–675. [CrossRef] [PubMed]

91. Delfs, J.R.; Dichter, M.A. Effects of somatostatin on mammalian cortical neurons in culture: Physiological actions and unusual dose response characteristics. *J. Neurosci.* **1983**, *3*, 1176–1188. [CrossRef]

92. Stornetta, R.L.; Rosin, D.L.; Wang, H.; Sevigny, C.P.; Weston, M.C.; Guyenet, P.G. A group of glutamatergic interneurons expressing high levels of both neurokinin-1 receptors and somatostatin identifies the region of the pre-Bötzinger complex. *J. Comp. Neurol.* **2003**, *455*, 499–512. [CrossRef]

93. Thek, K.R.; Ong, S.J.M.; Carter, D.C.; Bassi, J.K.; Allen, A.M.; McDougall, S.J. Extensive Inhibitory Gating of Viscerosensory Signals by a Sparse Network of Somatostatin Neurons. *J. Neurosci.* **2019**, *39*, 8038–8050. [CrossRef]

94. Cattaneo, S.; Zaghi, M.; Maddalena, R.; Bedogni, F.; Sessa, A.; Taverna, S. Somatostatin-Expressing Interneurons Co-Release GABA and Glutamate onto Different Postsynaptic Targets in the Striatum. *bioRxiv* **2019**, 566984. [CrossRef]

95. Kubota, Y.; Hattori, R.; Yui, Y. Three distinct subpopulations of GABAergic neurons in rat frontal agranular cortex. *Brain Res.* **1994**, *649*, 159–173. [CrossRef]

96. Kawaguchi, Y.; Kubota, Y. GABAergic cell subtypes and their synaptic connections in rat frontal cortex. *Cereb. Cortex* **1997**, *7*, 476–486. [CrossRef] [PubMed]

97. Xu, X.; Roby, K.D.; Callaway, E.M. Immunochemical characterization of inhibitory mouse cortical neurons: Three chemically distinct classes of inhibitory cells. *J. Comp. Neurol.* **2010**, *518*, 389–404. [CrossRef]

98. Xu, X.; Roby, K.D.; Callaway, E.M. Mouse cortical inhibitory neuron type that coexpresses somatostatin and calretinin. *J. Comp. Neurol.* **2006**, *499*, 144–160. [CrossRef]

99. Wang, Y.; Gupta, A.; Toledo-Rodriguez, M.; Wu, C.Z.; Markram, H. Anatomical, physiological, molecular and circuit properties of nest basket cells in the developing somatosensory cortex. *Cereb. Cortex* **2002**, *12*, 395–410. [CrossRef]

100. Riedemann, T.; Schmitz, C.; Sutor, B. Immunocytochemical heterogeneity of somatostatin-expressing GABAergic interneurons in layers II and III of the mouse cingulate cortex: A combined immunofluorescence/design-based stereologic study. *J. Comp. Neurol.* **2016**, *524*, 2281–2299. [CrossRef]

101. Wasilewska, B.; Robak, A.; Równiak, M.; Bogus-Nowakowska, K.; Najdzion, J.; Zakowski, W.; Majewski, M. Distribution and chemical coding pattern of somatostatin immunoreactivity in the dorsal striatum of the guinea pig. *Folia Histochem. Cytobiol.* **2011**, *49*, 690–699. [CrossRef]

102. Figueredo-Cardenas, G.; Morello, M.; Sancesario, G.; Bernardi, G.; Reiner, A. Colocalization of somatostatin, neuropeptide Y, neuronal nitric oxide synthase and NADPH-diaphorase in striatal interneurons in rats. *Brain Res.* **1996**, *735*, 317–324. [CrossRef]

103. Jinno, S.; Kosaka, T. Patterns of colocalization of neuronal nitric oxide synthase and somatostatin-like immunoreactivity in the mouse hippocampus: Quantitative analysis with optical disector. *Neuroscience* **2004**, *124*, 797–808. [CrossRef] [PubMed]

104. Post, R.J.; Warden, M.R. Depression: The search for separable behaviors and circuits. *Curr. Opin. Neurobiol.* **2018**, *49*, 192–200. [CrossRef]

105. Lin, L.C.; Sibille, E. Somatostatin, neuronal vulnerability and behavioral emotionality. *Mol. Psychiatr.* **2015**, *20*, 377–387. [CrossRef]

106. Noudoost, B.; Moore, T. The role of neuromodulators in selective attention. *Trends Cogn. Sci.* **2011**, *15*, 585–591. [CrossRef] [PubMed]

107. Khlghatyan, J.; Quintana, C.; Parent, M.; Beaulieu, J.M. High Sensitivity Mapping of Cortical Dopamine D2 Receptor Expressing Neurons. *Cereb. Cortex* **2019**, *29*, 3813–3827. [CrossRef]

108. Le Moine, C.; Normand, E.; Bloch, B. Phenotypical characterization of the rat striatal neurons expressing the D1 dopamine receptor gene. *Proc. Natl. Acad. Sci. USA* **1991**, *88*, 4205–4209. [CrossRef]

109. Engber, T.M.; Boldry, R.C.; Kuo, S.; Chase, T.N. Dopaminergic modulation of striatal neuropeptides: Differential effects of D1 and D2 receptor stimulation on somatostatin, neuropeptide Y, neurotensin, dynorphin and enkephalin. *Brain Res.* **1992**, *581*, 261–268. [CrossRef]

110. Mueller, A.; Krock, R.M.; Shepard, S.; Moore, T. Dopamine Receptor Expression Among Local and Visual Cortex-Projecting Frontal Eye Field Neurons. *Cereb. Cortex* **2020**, *30*, 148–164. [CrossRef]

111. Anastasiades, P.G.; Boada, C.; Carter, A.G. Cell-Type-Specific D1 Dopamine Receptor Modulation of Projection Neurons and Interneurons in the Prefrontal Cortex. *Cereb. Cortex* **2019**, *29*, 3224–3242. [CrossRef]

112. Adesnik, H.; Bruns, W.; Taniguchi, H.; Huang, Z.J.; Scanziani, M. A neural circuit for spatial summation in visual cortex. *Nature* **2012**, *490*, 226–231. [CrossRef]

113. Chen, S.X.; Kim, A.N.; Peters, A.J.; Komiyama, T. Subtype-specific plasticity of inhibitory circuits in motor cortex during motor learning. *Nat. Neurosci.* **2015**, *18*, 1109–1115. [CrossRef] [PubMed]

114. Gotti, C.; Zoli, M.; Clementi, F. Brain nicotinic acetylcholine receptors: Native subtypes and their relevance. *Trends Pharmacol. Sci.* **2006**, *27*, 482–491. [CrossRef]

115. Sun, Q.; Li, X.; Ren, M.; Zhao, M.; Zhong, Q.; Ren, Y.; Luo, P.; Ni, H.; Zhang, X.; Zhang, C.; et al. A whole-brain map of long-range inputs to GABAergic interneurons in the mouse medial prefrontal cortex. *Nat. Neurosci.* **2019**, *22*, 1357–1370. [CrossRef]

116. Obermayer, J.; Heistek, T.S.; Kerkhofs, A.; Goriounova, N.A.; Kroon, T.; Baayen, J.C.; Idema, S.; Testa-Silva, G.; Couey, J.J.; Mansvelder, H.D. Lateral inhibition by Martinotti interneurons is facilitated by cholinergic inputs in human and mouse neocortex. *Nat. Commun.* **2018**, *9*, 4101. [CrossRef] [PubMed]

117. Demars, M.P.; Morishita, H. Cortical parvalbumin and somatostatin GABA neurons express distinct endogenous modulators of nicotinic acetylcholine receptors. *Mol. Brain* **2014**, *7*, 75. [CrossRef]

118. Krubitzer, L.; Campi, K.L.; Cooke, D.F. All rodents are not the same: A modern synthesis of cortical organization. *Brain Behav. Evol.* **2011**, *78*, 51–93. [CrossRef]

119. Campi, K.L.; Krubitzer, L. Comparative studies of diurnal and nocturnal rodents: Differences in lifestyle result in alterations in cortical field size and number. *J. Comp. Neurol.* **2010**, *518*, 4491–4512. [CrossRef] [PubMed]

120. Kaas, J.H.; Hall, W.C.; Diamond, I.T. Visual cortex of the grey squirrel (*Sciurus carolinensis*): Architectonic subdivisions and connections from the visual thalamus. *J. Comp. Neurol.* **1972**, *145*, 273–305. [CrossRef]

121. Heimel, J.A.; Van Hooser, S.D.; Nelson, S.B. Laminar organization of response properties in primary visual cortex of the gray squirrel (*Sciurus carolinensis*). *J. Neurophysiol.* **2005**, *94*, 3538–3554. [CrossRef] [PubMed]

122. Van Hooser, S.D.; Heimel, J.A.; Chung, S.; Nelson, S.B.; Toth, L.J. Orientation selectivity without orientation maps in visual cortex of a highly visual mammal. *J. Neurosci.* **2005**, *25*, 19–28. [CrossRef] [PubMed]

123. Van Hooser, S.D.; Heimel, J.A.; Nelson, S.B. Functional cell classes and functional architecture in the early visual system of a highly visual rodent. *Prog. Brain Res.* **2005**, *149*, 127–145. [CrossRef]

124. Ferreiro, D.N.; Conde-Ocazionez, S.A.; Patriota, J.H.N.; Souza, L.C.; Oliveira, M.F.; Wolf, F.; Schmidt, K.E. Spatial clustering of orientation preference in primary visual cortex of the large rodent agouti. *iScience* **2021**, *24*, 101882. [CrossRef] [PubMed]

125. Bennett-Clarke, C.A.; Joseph, S.A. Immunocytochemical localization of somatostatin in human brain. *Peptides* **1986**, *7*, 877–884. [CrossRef]

126. Reubi, J.C.; Probst, A.; Cortes, R.; Palacios, J.M. Distinct topographical localisation of two somatostatin receptor subpopulations in the human cortex. *Brain Res.* **1987**, *406*, 391–396. [CrossRef]

127. Selmer, I.-S.; Schindler, M.; Humphrey, P.P.A.; Waldvogel, H.J.; Faull, R.L.M.; Emson, P.C. First localisation of somatostatin sst4 receptor protein in selected human brain areas: An immunohistochemical study. *Mol. Brain Res.* **2000**, *82*, 114–125. [CrossRef]

128. Mengod, G.; Rigo, M.; Savasta, M.; Probst, A.; Palacios, J.M. Regional distribution of neuropeptide somatostatin gene expression in the human brain. *Synapse* **1992**, *12*, 62–74. [CrossRef]

129. Thoss, V.S.; Pérez, J.; Probst, A.; Hoyer, D. Expression of five somatostatin receptor mRNAs in the human brain and pituitary. *Naunyn-Schmiedebergs Arch. Pharmacol.* **1996**, *354*, 411–419. [CrossRef]

130. Lewis, D.A.; Sweet, R.A. Schizophrenia from a neural circuitry perspective: Advancing toward rational pharmacological therapies. *J. Clin. Investig.* **2009**, *119*, 706–716. [CrossRef]